



Published in final edited form as:

*J Phys Chem B*. 2012 June 14; 116(23): 6936–6944. doi:10.1021/jp3002383.

## Simple liquid models with corrected dielectric constants

Christopher J. Fennell, Libo Li, and Ken A. Dill

Laufer Center for Physical and Quantitative Biology, Stony Brook University, Stony Brook, NY 11794

### Abstract

Molecular simulations often use explicit-solvent models. Sometimes explicit-solvent models can give inaccurate values for basic liquid properties, such as the density, heat capacity, and permittivity, as well as inaccurate values for molecular transfer free energies. Such errors have motivated the development of more complex solvents, such as polarizable models. We describe an alternative here. We give new fixed-charge models of solvents for molecular simulations – water, carbon tetrachloride, chloroform and dichloromethane. Normally, such solvent models are parameterized to agree with experimental values of the neat liquid density and enthalpy of vaporization. Here, in addition to those properties, our parameters are chosen to give the correct dielectric constant. We find that these new parameterizations also happen to give better values for other properties, such as the self-diffusion coefficient. We believe that parameterizing fixed-charge solvent models to fit experimental dielectric constants may provide better and more efficient ways to treat solvents in computer simulations.

### Keywords

Permittivity; Carbon Tetrachloride; Chloroform; Dichloromethane; Water

## 1 Introduction

In molecular simulations, solvents such as water are often represented by explicit models such as TIP3P or SPC.<sup>1,2</sup> Many of these explicit-solvent models were originally developed and parameterized a few decades ago. They were parameterized to agree with experimental data such as the density and enthalpy of vaporization of the neat liquid, key quantities that are readily available from accurate experiments. However, such molecular solvent models don't typically predict the correct experimental value of the dielectric constant.<sup>3–7</sup> This is unfortunate because molecular simulations are so commonly used to treat the solvation of polar and charged molecules, for which it is essential that the solvent respond properly to electrostatic fields. Reproducing the dielectric constant is especially critical in low-dielectric solvents like chloroform or cyclohexane. While solvents with dielectric constants of 80 and 60 can give solvation free energies of a charge within 1% of one another, solvents with dielectric constants of 2 and 1.5 will give solvation free energies that are more than 50% different.

When current solvent models fail to reproduce the dielectric constant, it is often concluded that improvement can only be achieved by resorting to more complicated geometries or additional interactions, such as those present in expensive polarizable or quantum chemical

\*Corresponding author. cfennell@gmail.com.

**Supporting Information Available** Model structural comparisons and full tables of temperature dependent property data can be found in the related supporting information. This information is available free of charge via the Internet at <http://pubs.acs.org>.

models.<sup>5,6,8-15</sup> We take a different approach here. Here, we develop classical fixed-charge molecular solvent models for water, CCl<sub>4</sub>, CHCl<sub>3</sub>, and CH<sub>2</sub>Cl<sub>2</sub>, but we parameterize them based on experimental dielectric constants, in addition to the solvent density and enthalpy of vaporization. We find that our newly parameterized solvent models capture some additional experimental properties at least as well as previous models, in addition to getting the dielectric constant correct. The benefit of re-parameterized fixed-charge models is that it allows for much more efficient simulations than those involving polarizable or QM forcefields.

We develop molecular models of carbon tetrachloride ( $\epsilon(0) = 2.2$  at 298.15 K and 1 atm), chloroform ( $\epsilon(0) = 4.7$ ), dichloromethane ( $\epsilon(0) = 8.9$ ), and water ( $\epsilon(0) = 78.4$ ). Our choice of which solvents to model was based on wanting a wide range of dielectric constants and wanting no more than two primary atom types. The latter is so that we can test our parameterization methodology for incorporating experimental dielectric constant information without the extra complexity or additional parameters that would be needed for multi-atom-type solvents.

## 2 Methods

### 2.1 Building initial molecular structures

For the chloromethanes, we start with the gas-phase geometry, and for water we used both the gas-phase geometry as in TIP3P water<sup>1</sup> and the simplified tetrahedral geometry of SPC water.<sup>2</sup> As chloroform and dichloromethane contain three atom types, we chose to work with united-atom variants to simplify the liquids to two atom-types, and compare how well an optimized united-atom model reproduces experimental quantities relative to an existing all-atom model.

To start the model optimization process, we first need an initial set of parameters. These include Lennard-Jones (LJ)  $\sigma_{LJ}$  and  $\epsilon_{LJ}$  parameters for each atom-type, as well as an initial distribution of partial charges. For each of these, we chose experimentally derived or simple values. As the  $\sigma_{LJ}$  parameter corresponds to an atom size, we chose the Bondi radii as the initial LJ radius, or  $\sigma_{LJ}/2$ .<sup>16</sup> For united-atom sites in CH<sub>2</sub>Cl<sub>2</sub> and CHCl<sub>3</sub>, we calculated the initial van der Waals volume of the all-atom versions of these molecules using a mutual overlapping spheres procedure.<sup>17</sup> We then placed the united-atom (UA) site at the center-of-mass of the carbon and hydrogen atoms and scaled the size of this UA site until the new volume of the molecule was equal to the all-atom van der Waals volume (see Fig. 1). As these molecules consist of only two atom-types, we distributed charges evenly amongst like atoms in accordance with the experimentally determined gas-phase molecular dipole moments. Finally, there are several avenues that one could take for assigning  $\epsilon_{LJ}$  parameters for atom-types. The  $\epsilon_{LJ}$  parameter corresponds to an atom's dispersion attraction, and one could assign relative depths based on polarizability, electronegativity, or even the number of valence electrons.<sup>18</sup> We have opted for the simpler route of assigning the same  $\epsilon_{LJ}$  value to all atom-types.

### 2.2 Optimization procedure

The typical route for developing molecular models for liquid simulations is to focus on matching the density, enthalpy of vaporization ( $\Delta H_{\text{vap}}$ ), and possibly another property like the self-diffusion coefficient or liquid structure.<sup>1-3,6,7,10,19-21</sup> Here we aim for agreement also with the dielectric constant, in addition to the experimental density and  $\Delta H_{\text{vap}}$ . To show how these molecular models can be made to agree with these experimental quantities, we uniformly scaled the  $\sigma_{LJ}$  values, charge magnitudes, and  $\epsilon_{LJ}$  values and calculated how the properties changed. An example illustrating how scaling of these parameters affects these

properties is shown in Fig. 2. Starting from the constructed united-atom  $\text{CH}_2\text{Cl}_2$  model, it is apparent that both the density ( $\rho$ ) and dielectric constant ( $\epsilon(0)$ ) are sharply dependent upon the size of the molecule. However, when the chargemagnitudes ( $q$ ) are uniformly scaled, the dielectric constant is effected to a much greater degree than the density. Finally,  $\epsilon_{\text{LJ}}$  changes primarily affect the  $\Delta H_{\text{vap}}$  mostly independent of the other properties. This gives a prescription for sequential optimization of the model parameters for fitting to the experimental properties of interest.

1. Fit  $\rho$  by uniformly scaling all the  $\sigma_{\text{LJ}}$  values
2. Fit  $\epsilon(0)$  by uniformly scaling all the  $q$  values
3. Fit  $\Delta H_{\text{vap}}$  by uniformly scaling all the  $\epsilon_{\text{LJ}}$  values

Each step of this optimization process involves a linear fitting procedure in the specific parameter space of interest. For example, the initial process of fitting the density involves an initial simulation with the starting set of parameters and a check to see if it is greater or less than the target value. If the liquid is too dense, the  $\sigma_{\text{LJ}}$  values are all increased by 5% to expand the system, and the density is recomputed after another simulation. We then linearly interpolate to find the  $\sigma_{\text{LJ}}$  scaling that corresponds to the target density. Since the relations between properties and parameters are not strictly linear, multiple interpolation steps using the current and previous step information are often needed to fit a given parameter.

Typically, we see convergence on a given property to a specified tolerance within 2 to 4 interpolation steps.

It is apparent in Fig. 2 that the liquid properties are not exclusively dependent upon single model parameters – changing one of the parameters will have some effect on all of the properties. This means that this sequence needs to be iterated to focus in on the optimal set of experimental properties. The amount of iteration depends on the degree to which the parameters are correlated with the properties and the width of the specified tolerances. Table 1 lists the target properties for all the liquids and fitting tolerance for each. For the chloromethanes, convergence was typically achieved within 2 or 3 iterations. Water properties tended to be more correlated to the model parameters, so 5 or more iterations were not uncommon.

Solutions found by this optimization procedure are not necessarily unique, particularly given that there is an allowed tolerance window for each property. Despite this, multiple optimizations involving different initial dipole moments all ended with similar final parameters.

### 2.3 $\text{CCl}_4$ poses a challenge

$\text{CCl}_4$  poses an interesting challenge for our present approach.  $\text{CCl}_4$  is tetrahedral and symmetric. It has no dipole moment in the gas-phase. Without a dipole moment, a rigid fixed-charge liquid model will have a dielectric constant  $\epsilon(0)$  close to 1. Yet,  $\text{CCl}_4$  has a dielectric response ( $\epsilon(0) > 2$ ). It and other non-polar liquids have apparent dipolar character in the liquid state.<sup>23</sup> This situation has motivated the recent development of polarizable models for  $\text{CCl}_4$  and for other low-dielectric liquids.<sup>14,15</sup> In order to retain the advantages of fixed-charge force fields, our approach here instead is to include a permanent dipole in the model. Such a dipole moment will likely be different than an experimentally measured dipole moment for  $\text{CCl}_4$  as it will incorporate the polarizable contributions to the permittivity.

There are different ways to incorporate a dipole in  $\text{CCl}_4$ . We explored all the possibilities for distributing the positive and negative partial charges of a dipole throughout the atoms in a molecule having this symmetry. All models successfully fit the experimental data and

exhibited identical experimental properties that were not part of the fitting procedure. In the interest of simplicity, we only discuss two of the models, illustrated in Fig. 3. In these models, the dipole is either localized along one of the C-Cl bonds or distributed across three of them. All plotted data below is from the simpler localized model (Fig. 3a).

## 2.4 Simulation details

All molecular dynamics calculations were performed using version 4.5.5 of the GROMACS molecular dynamics package.<sup>24,25</sup> The leap-frog algorithm with time steps of 4 fs for chloromethane and 2 fs for water simulations were used to integrate the equations of motion. The chloromethane models were held rigid using the SHAKE algorithm,<sup>26</sup> while the water models were held rigid using the SETTLE algorithm.<sup>27</sup> The isothermal-isobaric ensemble (*NPT*) using the Nose-Hoover thermostat and the Parrinello-Rahman barostat was used in both the optimization and temperature dependent property simulations. Dynamical properties were also computed from these simulations, and these properties were independently verified with sets of microcanonical (*NVE*) ensemble simulations. Long-range electrostatics were handled using the smooth version of the particle mesh Ewald (PME) method<sup>28</sup> under tin-foil boundary conditions with a grid spacing of 0.12, a PME order of 4, an Ewald parameter energy tolerance of  $10^{-5}$ , and a real-space cutoff of 15 Å for chloromethane and 12 Å for water simulations. The Lennard-Jones (LJ) interactions were switched off from 10 to 12 Å for the chloromethane and 8 to 10 Å for water simulations, and energy and pressure tail corrections were included in all cases. As seen by others,<sup>29,30</sup> the longer LJ cutoff is necessary to achieve converged system densities. Lorentz-Berthelot mixing rules were used to compute mixed-LJ interactions between differing atom types.

Optimization simulations involved rhombic dodecahedral boxes of 325 molecules for chloromethane simulations and cubic boxes of 650 molecules for water simulations. All of these simulations were carried out at 298.15 K and 1 atm. Run-time lengths ranged from 1 ns for density and  $\Delta H_{\text{vap}}$  optimization to 10 ns for  $\epsilon(0)$  optimization. System size effects were investigated with the final parameter sets by calculating properties for systems with four times the number of atoms with increasingly larger interaction cutoff radii, and property results were identical within error to those from these smaller systems. The calculated final properties are averages from five independent 10 ns simulations, and standard errors are reported for these averages. For the water models, we also extended the 298.15 K simulations out to 50 ns to test the convergence of  $\epsilon(0)$ . All calculated properties for water at 298.15 K come from these longer simulations.

## 2.5 Calculation of liquid properties

With proper sampling of the given ensemble, thermodynamic and dynamic properties can be computed from fluctuations over the course of the simulation. In addition to the density, the following properties were calculated for all the optimized models.

**2.5.1 Enthalpy of vaporization**—The enthalpy of vaporization is traditionally computed from the difference between the enthalpy of an ideal gas and the liquid state,

$$\Delta H_{\text{vap}}(T) = H(T)_{\text{ideal}} - H(T)_{\text{liq}} = -\langle E_{\text{liq}} \rangle / N + RT, \quad (1)$$

where  $E_{\text{liq}}$  is the total intermolecular energy of the system of  $N$  molecules,  $R$  is the ideal gas constant, and  $T$  is the temperature. Others have noted that more detailed estimations of  $\Delta H_{\text{vap}}$  can be determined by including non-classical and non-ideal gas corrections.<sup>6</sup> We decided to use the traditional approximation as it corresponds to the heat required to vaporize these non-polarizable models in simulations, though including such corrections could lead to improved agreement with experimental properties.

**2.5.2 Static dielectric constant**—For non-polarizable liquids,  $\epsilon(0)$  can be calculated from fluctuations of the total system dipole moment ( $\mathbf{M}$ ) according to,

$$\epsilon(0) = 1 + \frac{4\pi}{3k_B T \langle V \rangle} (\langle M^2 \rangle - \langle M \rangle^2), \quad (2)$$

where  $k_B$  is the Boltzmann constant and  $V$  is the total system volume.<sup>31</sup> One difficulty in calculating  $\epsilon(0)$  is that it is accumulated as a running average and will typically not converge over subnanosecond simulations. We needed to perform 10 ns simulations in order to obtain consistent estimates of  $\epsilon(0)$  for all liquids.

**2.5.3  $C_p$ ,  $\kappa_T$ , and  $\alpha_p$** —As an additional test of thermodynamic quantities for the resulting models, we computed the isobaric heat capacity ( $C_p$ ), the isothermal compressibility ( $\kappa_T$ ), and the thermal expansion coefficient ( $\alpha_p$ ). These were calculated using the following fluctuation formulae from  $NPT$  simulations,

$$C_p = \left( \frac{\partial H}{\partial T} \right)_{N,P} = \frac{\langle H^2 \rangle - \langle H \rangle^2}{Nk_B T^2} + 3R, \quad (3)$$

$$\kappa_T = -\frac{1}{V} \left( \frac{\partial V}{\partial P} \right)_{N,T} = \frac{\langle V^2 \rangle - \langle V \rangle^2}{k_B T \langle V \rangle}, \quad (4)$$

$$\alpha_p = \frac{1}{V} \left( \frac{\partial V}{\partial T} \right)_{N,P} = \frac{\langle VH \rangle - \langle V \rangle \langle H \rangle}{k_B T^2 \langle V \rangle}. \quad (5)$$

**2.5.4 Self-diffusion coefficient**—The self-diffusion coefficient was calculated for all the models alongside the above thermodynamic quantities.  $D$  was calculated from a regression fit to the linear region (0.5–6 ns) of a plot of the Einstein relation,<sup>32</sup>

$$D = \lim_{t \rightarrow \infty} \frac{\langle |\mathbf{r}_i(t) - \mathbf{r}_i(0)|^2 \rangle}{6t}, \quad (6)$$

where  $\mathbf{r}_i(t)$  is the position of the center of mass of molecule  $i$  at time  $t$ . Dynamical quantities are typically calculated from  $NVE$  simulations in order to avoid perturbations introduced by thermostats and barostats. We calculated  $D$  for all models from  $NVE$  simulations near 298.15 K and 1 atm, and found that they were identical to the  $NPT$  simulations used for the above thermodynamic quantities. This indicated that the thermostat and barostat coupling was weak enough to not significantly perturb the dynamics. We report  $D$  results from the  $NPT$  simulations for simplicity.

**2.5.5 Structural analysis**—Finally, we calculated radial distribution functions between various atom types for comparisons with other models and experimental scattering data. These distribution functions were calculated by binning separation distances ( $r_{ij}$ ) between atoms of type  $A$  and  $B$  via

$$g_{AB}(r) = \frac{1}{N_A \langle \rho_B \rangle} \sum_{i \in A} \sum_{j \in B} \frac{\delta(r_{ij} - r)}{4\pi r^2}, \quad (7)$$

where  $\rho_B$  is the bulk system density of atom type  $B$ .

### 3 Results and Discussion

Table 2 gives the values of our parameters for the non-polar solvents we modeled. And, Table 3 compares the properties we calculate from our models compared to all-atom RESP models from Fox & Kollman<sup>30</sup> and to experiments. The models from the present work are labelled with DC, to indicate that they are ‘dielectric corrected’. The Fox models are flexible all-atom models – they allow harmonic bond stretching and angle bending motions – that are derived from the AMBER force field.<sup>33</sup> The values reported here differ considerably from those published (specifically the self-diffusion constant). This difference comes from the expanded sampling in these simulations that provide a better estimate of the actual thermodynamic and dynamic properties of the models.

All the DC models shown in Table 3 are converged on the experimental density,  $\Delta H_{\text{vap}}$ , and dielectric constant to within the previously stated tolerances. The dielectric constant was the slow step in the fitting process. Fig. 4 shows the running average of the  $\epsilon(0)$  values, over the course of 10 ns of molecular dynamics. The lines are average traces over five simulations, and the shaded region shows the standard deviation of these averages. While the dielectric constant of  $\text{CCl}_4$  levels quickly and the deviations are barely visible, the  $\text{CH}_2\text{Cl}_2$  trace shows the difficulty in fitting when considering liquids with higher dielectric constants. At the end of the 10 ns, the standard deviation is still roughly  $\pm 0.2$  dielectric units, very close to the size of our tolerance window for convergence. To fit the dielectric to a tighter window, we would need proportionally longer simulation times. If we wanted to work with a material with a larger dielectric constant, we would either need a looser  $\epsilon(0)$  convergence criterion or longer simulation lengths.

#### 3.1 Adding a dipole improves the permittivity of $\text{CCl}_4$

In Table 3, there is a noticeable trend of increasing dipole moment with increasing  $\epsilon(0)$  from  $\text{CCl}_4$  down to  $\text{CH}_2\text{Cl}_2$ . This trend has been recognized in the past,<sup>5,21,38</sup> and it simply follows that the greater the partial charges, the greater the screening ability of the liquid. This results holds true for the flexible all-atom models as well, as they have lower average dipole moments than the analogous DC models and consistently under-predict the dielectric constant. In the case of  $\text{CCl}_4$ , the embedded dipole actually allows the DC models to express a  $\epsilon(0)$  in line with experiment. Both the thermodynamic and dynamic properties are nearly identical for the localized and distributed  $\text{CCl}_4$  models, as are the dipole moments for the two models. These results indicate that the geometry of the charge distribution that makes the dipole moment is less important than the magnitude.

As the  $\text{CCl}_4$ -DC models are fit to experimental density,  $\Delta H_{\text{vap}}$ , and  $\epsilon(0)$  quantities, it is not surprising that they reproduce these quantities better than the all atom model. The Fox & Kollman model captured a small fraction of the permittivity as it is flexible and has a small dipole moment in the liquid phase. While the diffusivity relative to experiment for  $\text{CCl}_4$ -DC is improved over the flexible model, the  $a_p$  for the  $\text{CCl}_4$ -DC models is considerably degraded. Embedding a dipole had the effect of increasing the  $\sigma_{\text{LJ}}$  values on the atoms, and this makes the volume of the liquid more sensitive to temperature changes. This results in the liquid having a less tightly structured first solvation shell than the flexible Fox & Kollman model (see Supporting Information) and a possibly less accurate fit to neutron scattering experiments.<sup>39</sup>

### 3.2 United-atom chloromethanes behave similarly to all-atom models

In addition to corrected dielectric versions of these liquids, we were interested in united-atom variants of  $\text{CHCl}_3$  and  $\text{CH}_2\text{Cl}_2$  that could work as a more efficient mimic of a detailed all-atom model. The results in Table 3 indicate this to be the case. Not surprisingly, the DC models fit well the experimental data to which they were matched. More interesting, however, is the observation that these new models do well at reproducing other thermodynamic properties of the real liquid that were not part of the parameterization exercise, often better than the more detailed Fox & Kollman models. While structural comparisons between united-atom and all-atom models are inexact, a qualitative radial distribution function comparison indicates that both  $\text{CHCl}_3$ -DC and  $\text{CH}_2\text{Cl}_2$ -DC are more structured than the flexible all-atom Fox & Kollman models (see Supporting Information). This is likely due to the enhanced dipole moments of the dielectric corrected models, resulting in stronger pair interactions and larger  $\Delta H_{\text{vap}}$  values. These results indicate that even with a less complex model geometry, correcting for the dielectric has additional advantages.

### 3.3 The DC chloromethane models capture some of the temperature dependence of $\epsilon(0)$

These DC models, like other liquid models, are fit to one temperature. We tested how well our DC models capture the temperature dependence of the dielectric constant, in 5 K increments within the available range of experimental data for  $\epsilon(0)$ ; see Fig. 5. At the fitting temperature of 298.15 K, all the models match with experiments. All the models have the correct sign of the slope:  $\epsilon(0)$  decreases with increasing temperature. At low temperatures, the  $\text{CH}_2\text{Cl}_2$  and  $\text{CHCl}_3$  models deviate from the experimental  $\epsilon(0)$  values, while the  $\text{CCl}_4$ -DC model results (localized dipole model shown in Fig. 5) are quantitative across the entire available range.

### 3.4 Applying the dielectric correction to water models

We were interested to see if we could improve upon current water models, by correcting their dielectric constants in the manner described above. We considered two water models: TIP3P ( $\epsilon(0) > 90$ ) and SPC ( $\epsilon(0) < 70$ ).<sup>40</sup>

The atom sites in TIP3P are arranged in the experimental gas-phase geometry, and from a property standpoint, the density is less than experiment and  $\epsilon(0)$  is greater than experiment. We would therefore expect both the  $\sigma$  parameter and charge magnitudes to decrease in order to align with experiment. Indeed these changes occur; however, the intermediate models rapidly crystallize into face-centered cubic lattices. We tested multiple starting states (larger and smaller  $\sigma$  and  $q$  values), and this crystallization was repeatable in all cases. Weakening the electrostatic interaction in TIP3P to match the experimental  $\epsilon(0)$  eliminates its ability to effectively hydrogen-bond. This observation appears to agree with findings showing alteration of the bond-angle of SPC/E below  $105^\circ$  (the bond-angle of TIP3P is  $104.5^\circ$ ) and above  $115^\circ$  causes a breakdown in the liquid properties.<sup>41,42</sup> This also corresponds to how other researchers have been successful in modifying the TIP4P model to better reproduce liquid and phase behavior properties.<sup>6,7</sup> By having the negative partial charge offset from the Lennard-Jones site center, TIP4P models are effectively more tetrahedral than the gas-phase geometry suggests.

The atom sites in SPC are perfectly tetrahedral, and the dielectric correction procedure was able to converge on a liquid-state model. The resulting parameters for SPC/DC are listed in Table 4. In addition to this SPC geometry based model, we show the resulting parameters for a tetrahedral model that has O–H bond lengths equal to the experimental gas-phase value (also the TIP3P value). We refer to this model as  $\text{H}_2\text{O}$ -DC, and it is a hybrid water model that probes both how SPC would respond to having bond-lengths in better agreement with

experiment and how TIP3P would respond with a more tetrahedral geometry. Properties at 298.15 K and 1 atm are listed in Table 5 alongside those for SPC, SPC/E, and experiment.

### 3.5 Optimized SPC resembles models with lower dielectric constants

When the SPC/E water model was originally developed, the authors recognized the need for an added extended polarization interaction to the SPC model.<sup>19</sup> They incorporated this effect by uniformly increasing the charge magnitude on the atom sites, keeping all other model parameters the same. This changed the dipole moment from 2.27 D to 2.35 D and subsequently improved most of the structural, thermodynamic, and dynamic properties. This increase in the dipole moment is the maximum possible without increasing the density of the liquid above 1 g/cm<sup>3</sup>. One point of note shown in Table 5 is the increase in  $\epsilon(0)$  from 66 to 71. To bring the SPC model  $\epsilon(0)$  up to the experimental value, the charge magnitudes need to be scaled up further, and the other model parameters (namely  $\sigma$  and  $\epsilon$ ) will need to be simultaneously adjusted to compensate for the increasing density. The resulting SPC/DC model parameters shown in Table 4 do exactly this. The oxygen site charge increases from 0.82 to 0.8476 to 0.87362 for SPC, SPC/E, and SPC/DC respectively, and the LJ parameters are modified to accommodate this additional charge. Fig. 6 shows the convergence of  $\epsilon(0)$  over the course of 50 ns of molecular dynamics. These traces further emphasize the difficulty in converging on a specific  $\epsilon(0)$  when working with high dielectric liquids. The standard deviation spread for SPC/DC has reached the  $\pm 1.5$  dielectric unit tolerance by 10 ns, though the dielectric optimization process would likely be more efficient using longer simulations for more accurate intermediate assessments of  $\epsilon(0)$ .

Table 5 shows that our dielectric correction leads to minor improvements of agreement with experiments for most of the thermodynamic and dynamic quantities, compared to SPC/E. Fig. 7 shows that the  $g_{OO}(r)$ ,  $g_{OH}(r)$ , and  $g_{HH}(r)$  for these three water models are nearly superimposable. The SPC and SPC/DC  $g(r)$  curves fall right on top of one another in all three plots, while the SPC/E curves are more peaked and have a slightly more ordered second-shell. This is likely a degradation in the overall liquid structure as the SPC/E model has been shown to be a better fit to neutron and x-ray scattering data.<sup>44-46</sup>

One possible consideration in matching experimental structural data is the geometry of the particular model. For the SPC models, the OH bond-length was simplified to 1 Å, while experimental structural data recommends a value closer to 0.958 Å.<sup>47</sup> Taking this geometry consideration into account, we developed and optimized a tetrahedral model with these OH bond-lengths that we call H<sub>2</sub>O-DC. While this model has a less converged  $\Delta H_{\text{vap}}$  than SPC/DC, it shows further improvements in most of the other liquid properties. By using shorter OH bond-lengths, we expect and observe some changes in the liquid structure. Fig. 8 shows the same sequence of radial distribution functions as Fig. 7, only with H<sub>2</sub>O-DC in place of SPC/DC. H<sub>2</sub>O-DC is slightly more structured beyond the first solvation shell than SPC/E in all of the curves. This structuring is more in line with scattering data,<sup>44-46,48</sup> making it a potentially truer representation of the real liquid. It should be noted that the first solvation shell for SPC/E type models is typically more peaked than the curves derived from model fits to this experimental scattering data, and this could likely be optimized by using a softer function for the van der Waals potential and/or decreasing the strength of the direct pair-interaction energy.

### 3.6 DC water models reproduce temperature dependent properties

We looked at the maximum in density as a function of temperature,  $T_{\text{max}}$  for these water models. This is experimentally observed at 277 K. Additional interaction sites have been added to some water models to capture this behavior.<sup>6,10</sup> SPC/E also has a  $T_{\text{max}}$ , though it is located around 235 K, well below the experimental melting point.<sup>49</sup>



Fig. 9 compares the predicted density-maximum temperatures from various models, spanning the supercooled-liquid and liquid phases. Here, the  $T_{max}$  for SPC/E is at 247 K. Our computation of this differs from past estimates, likely because the uses of the Ewald summation and LJ pressure correction were not as common when the original estimates were made.<sup>49</sup> As noted in past studies,<sup>52</sup> the SPC model does not exhibit a  $T_{max}$  in the temperature range shown, and interestingly, SPC/DC shows a density maximum (calculated from the sign crossover in  $\alpha_p$  seen in the supplementary materials) at 239 K, near the edge of the simulated temperature range. Thus, by adopting a liquid structure similar to SPC, this model shows a degradation in the  $T_{max}$  relative to SPC/E. The more structured H<sub>2</sub>O-DC has a  $T_{max}$  at 255 K, closer to experiment than SPC/E. This result indicates that it may be possible to optimize a rigid, 3-site water model through geometry distortions and interaction energy scaling to simultaneously reproduce both the  $\epsilon(0)$  and  $T_{max}$ .

Fig. 10 shows the temperature dependence of  $\epsilon(0)$ . The DC models reproduce the experimental  $\epsilon(0)$  at the optimization temperature and the correct trend of decreasing  $\epsilon(0)$  with increasing temperature, but not the slope quantitatively. All these models have the same slope, so correcting the dielectric constant at one temperature simply results in a vertical shift of the trend. More complex water models with different interaction site geometries have been shown to better capture the experimental slope,<sup>6,21</sup> so it may be useful in the future to couple changing molecular geometries with the present approach for correcting the dielectrics.

## 4 Conclusions

We have developed here parameters for solvents carbon tetrachloride, a united-atom chloroform, a united-atom dichloromethane, and water for molecular simulations in fixed-charge force fields. The usual approach to development is to choose parameters that cause the molecular simulations of the pure solvent to agree with experiments on the solvent density and enthalpy of vaporization. What's novel here is that our parameters are chosen so that the simulations also give the correct experimental dielectric constants. We find that our models also generally give better agreement with other properties, such as the self-diffusion constant. For water, there is some subtlety. When TIP3P is made to have the correct dielectric constant, it loses the appropriate level of water-water hydrogen bonding. However, when SPC is made to have the correct dielectric constant, it also has improved thermodynamic and dynamic properties. The present work indicates that the present approach to parameterizing fixed-charge solvent models for molecular simulations can improve the properties of those solvents relative to older parameterizations. And, this approach may circumvent the need, at least in some cases, to resort to more expensive polarizable or quantum mechanical solvent models.

## Supplementary Material

Refer to Web version on PubMed Central for supplementary material.

## Acknowledgments

We dedicate this paper to Harold Scheraga, who has been such an extraordinary pioneer, gentleman, and mentor to us and so many others. The authors gratefully acknowledge financial support provided by NIH grant GM63592.

## References

- [1]. Jorgensen WL, Chandrasekhar J, Madura JD, Impey RW, Klein ML. *J. Chem. Phys.* 1983; 79:926–935.

- [2]. Berendsen, HJC.; Postma, JPM.; van Gunsteren, WF.; Hermans, J. Simple Point Charge Water. In: Pullman, B., editor. *Intermolecular Forces*. Reidel; Dordrecht: 1981.
- [3]. van der Spoel D, van Maaren PJ, Berendsen HJC. *J. Chem. Phys.* 1998; 108:10220–10230.
- [4]. Jorgensen WL, Jenson C. *J. Comput. Chem.* 1998; 19:1179–1186.
- [5]. Guillot B. *J. Mol. Liq.* 2002; 101:219–260.
- [6]. Horn HW, Swope WC, Pitera JW, Madura JD, Dick TJ, Hura GL, Head-Gordon T. *J. Chem. Phys.* 2004; 120:9665–9678. [PubMed: 15267980]
- [7]. Abascal JLF, Vega C. *J. Chem. Phys.* 2005; 123:234505. [PubMed: 16392929]
- [8]. Rick SW, Stuart SA, Bader JS, Berne B. *J. Mol. Liq.* 1994; 65/66:31–40.
- [9]. Tironi G, Brunne RM, van Gunsteren WF. *Chem. Phys. Lett.* 1996; 250:19–24.
- [10]. Mahoney MW, Jorgensen WL. *J. Chem. Phys.* 2000; 112:8910–8922.
- [11]. Glättli A, Daura X, van Gunsteren WF. *J. Chem. Phys.* 2002; 116:9811–9828.
- [12]. Glättli A, Daura X, van Gunsteren WF. *J. Comput. Chem.* 2003; 24:1087–1096. [PubMed: 12759908]
- [13]. Wu Y, Tepper HL, Voth GA. *J. Chem. Phys.* 2006; 124:024503. [PubMed: 16422607]
- [14]. Lamoureux G, Faraldo-Gómez JD, Krupin S, Noskov SY. *Chem. Phys. Lett.* 2009; 468:270–274.
- [15]. Kunz A-PE, Eichenberger AP, van Gunsteren WF. *Mol. Phys.* 2011; 109:365–372.
- [16]. Bondi A. *J. Phys. Chem.* 1964; 68:441–451.
- [17]. Gibson KD, Scheraga HA. *J. Phys. Chem.* 1987; 91:4121–4122.
- [18]. Nagle J. *J. Am. Chem. Soc.* 1990; 112:4741–4747.
- [19]. Berendsen HJC, Grigera JR, Straatsma TP. *J. Phys. Chem.* 1987; 91:6269–6271.
- [20]. Liu H, Müller-Plathe F, van Gunsteren WF. *J. Am. Chem. Soc.* 1996; 117:4363–4366.
- [21]. Rick SW. *J. Chem. Phys.* 2004; 120:6085–6093. [PubMed: 15267492]
- [22]. Lide, DR., editor. *CRC Handbook of Chemistry and Physics*. 84 ed. CRC Press, Inc.; Boca Raton, FL: 2004.
- [23]. Garg SK, Bertie JE, Kilp H, Smyth CP. *J. Chem. Phys.* 1968; 49:2551–2562.
- [24]. Berendsen HJC, van der Spoel D, van Drunen R. *Comp. Phys. Comm.* 1995; 91:43–56.
- [25]. Hess B, Kutzner C, van der Spoel D, Lindahl E. *J. Chem. Theory Comput.* 2008; 4:435–447.
- [26]. Ryckaert J, Ciccotti G, Berendsen HJC. *J. Comput. Phys.* 1977; 23:327–341.
- [27]. Miyamoto S, Kollman PA. *J. Comput. Chem.* 1992; 13:952–962.
- [28]. Essman U, Perela L, Berkowitz ML, Darden T, Lee H, Pedersen LG. *J. Chem. Phys.* 1995; 103:8577–8592.
- [29]. Tironi IG, van Gunsteren WF. *Mol. Phys.* 1994; 83:381–403.
- [30]. Fox T, Kollman PA. *J. Phys. Chem. B.* 1998; 102:8070–8079.
- [31]. Neumann M. *Mol. Phys.* 1983; 50:841–858.
- [32]. Allen, MP.; Tildesley, DJ. *Computer Simulations of Liquids*. Oxford University Press; New York: 1987.
- [33]. Cornell WD, Cieplak P, Bayly CI, Gould IR, Merz KM Jr, Ferguson DM, Spellmeyer DC, Fox T, Caldwell JW, Kollman PA. *J. Am. Chem. Soc.* 1995; 117:5179–5197.
- [34]. Watts H, Alder BJ, Hildebrand JH. *J. Chem. Phys.* 1955; 23:659–661.
- [35]. Bender HJ, Zeidler MD. *Ber. Bunsen-Ges. Phys. Chem.* 1971; 75:236–242.
- [36]. Harris KR, Lam HN, Raedt E, Eastal AJ, Price WE, Woolf LA. *Mol. Phys.* 1990; 71:1205–1221.
- [37]. Brier PN, Perry A. *Adv. Mol. Relax. Inter. Processes.* 1978; 13:1–46.
- [38]. Sprik M. *J. Chem. Phys.* 1991; 95:6762–6769.
- [39]. Pusztai L, McGreevy RL. *Mol. Phys.* 1997; 90:533–539.
- [40]. van der Spoel D, van Maaren PJ. *J. Chem. Theory Comput.* 2006; 2:1–11.
- [41]. Höchtel P, Boresch S, Bitomsky W, Steinhauser O. *J. Chem. Phys.* 1998; 109:4927–4937.
- [42]. Chatterjee S, Debenedetti PG, Stillinger FH, Lynden-Bell RM. *J. Chem. Phys.* 2008; 128:124511. [PubMed: 18376947]

- [43]. Mills R. *J. Phys. Chem.* 1973; 77:685–688.
- [44]. Kusalik PG, Svishchev IM. *Science*. 1994; 265:1219–1221. [PubMed: 17787590]
- [45]. Sorenson JM, Hura G, Glaeser RM, Head-Gordon T. *J. Chem. Phys.* 2000; 113:9149–9161.
- [46]. Hura G, Russo D, Glaeser RM, Head-Gordon T, Krack M, Parrinello M. *Phys. Chem. Chem. Phys.* 2003; 5:1981–1991.
- [47]. Hoy AR, Bunker PR. *J. Mol. Spec.* 1979; 74:1–8.
- [48]. Soper AK, Phillips MG. *Chem. Phys.* 1986; 107:47–60.
- [49]. Báez LA, Clancy P. *J. Chem. Phys.* 1994; 101:9837–9840.
- [50]. Kell GS. *J. Chem. Eng. Data.* 1975; 20:97–105.
- [51]. Wagner W, Pruss A. *J. Phys. Chem. Ref. Data.* 2002; 31:387–535.
- [52]. Billeter SR, King PM, van Gunsteren WF. *J. Chem. Phys.* 1994; 100:6692–6699.

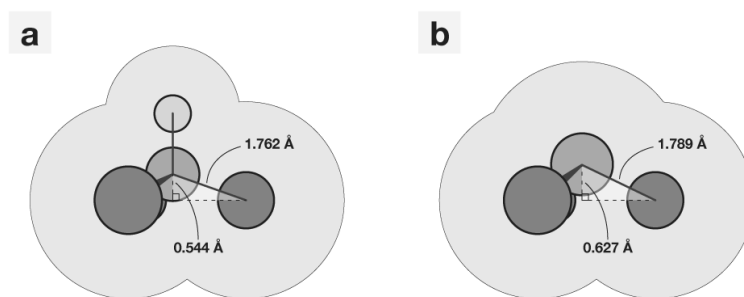


**Figure 1.** The (a) initial gas-phase geometry representation of chloroform and (b) the resulting united atom representation.

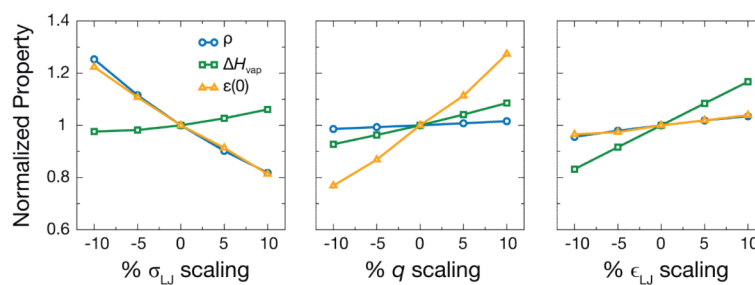


**Figure 2.**

The variation of the normalized density ( $\rho$ ), enthalpy of vaporization ( $\Delta H_{\text{vap}}$ ), and dielectric constant ( $\epsilon(0)$ ) of  $\text{CH}_2\text{Cl}_2$  as a function of uniform parameter variation. As the LJ  $\sigma_{\text{LJ}}$  (left) is scaled, both  $\rho$  and  $\epsilon(0)$  sharply vary. When the charge magnitude (middle) and LJ  $\epsilon_{\text{LJ}}$  (right) are scaled, only  $\epsilon(0)$  and only  $\Delta H_{\text{vap}}$  sharply vary respectively.

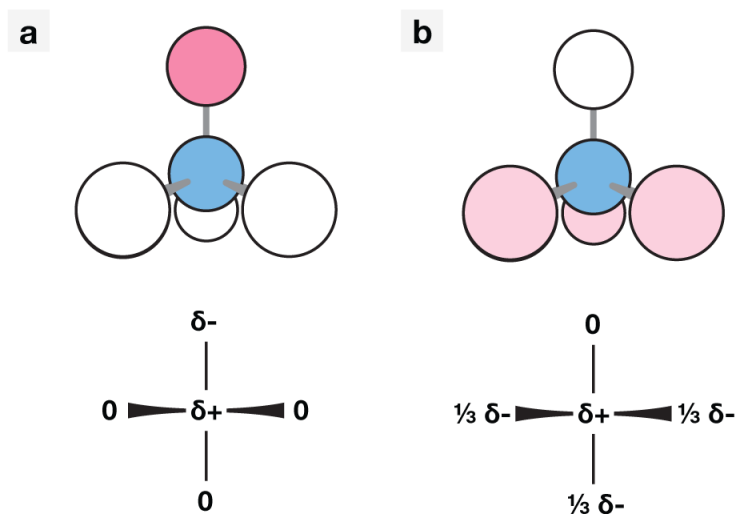


**Figure 3.** The (a) localized and (b) distributed dipole models for  $\text{CCl}_4$ . The localized model places the positive charge on the carbon atom and the negative on a single chlorine, while the distributed model splits the negative charge over three of the chlorine atoms.

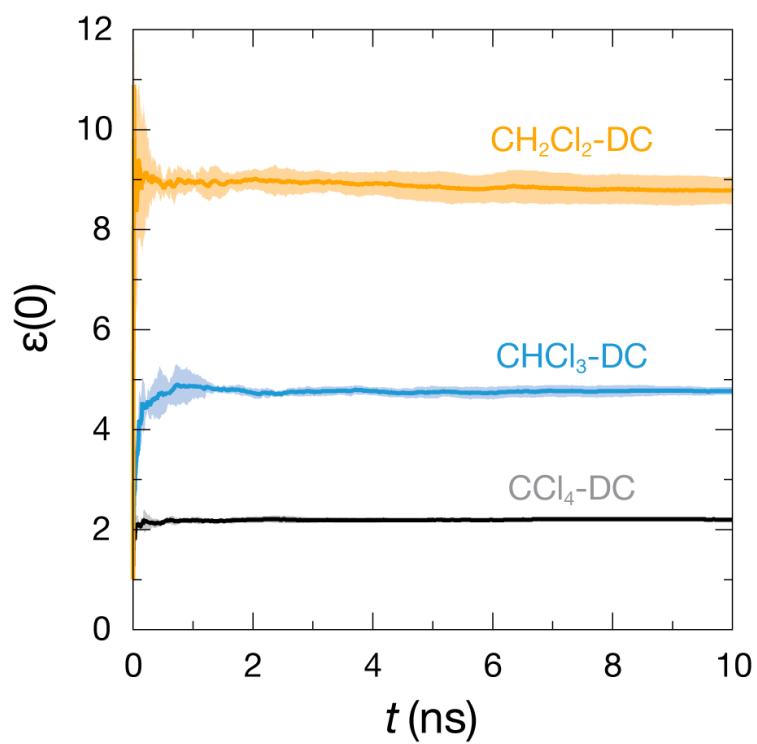


**Figure 4.** The static dielectric constant for the DC chloromethane models over the course of 10 ns of molecular dynamics at 298.15 K and 1 atm. The lines are averages of five simulations, and the shaded regions show the standard deviation of these averages.

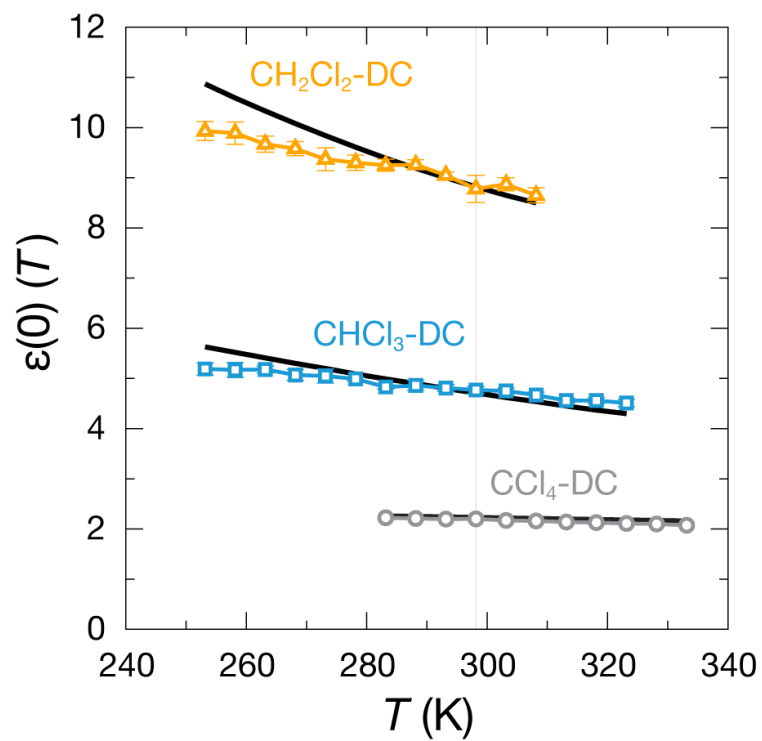


**Figure 5.** The temperature dependence of  $\epsilon(0)$  for the DC chloromethane models compared with experimental data.<sup>22</sup> The black lines are the experimental curves for each liquid shown.



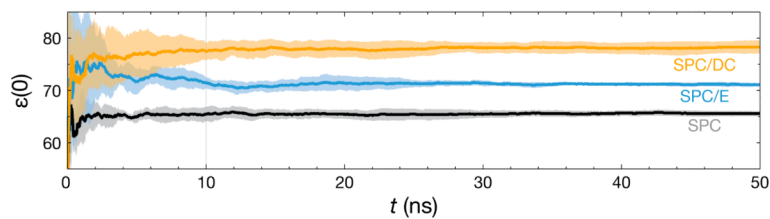


**Figure 6.** The static dielectric constant for SPC (black line), SPC/E (blue line), and SPC/DC (gold line) over the course of 50 ns of molecular dynamics at 298.15 K and 1 atm. The lines are averages of five simulations, and the shaded regions show the standard deviation of these averages. The plots show that the models have difficulty converging  $\epsilon(0)$  on time-scales less than 10 ns, the length of simulations in our dielectric correction procedure. Longer simulations would likely aid in optimization processes set to converge on a high  $\epsilon(0)$ .

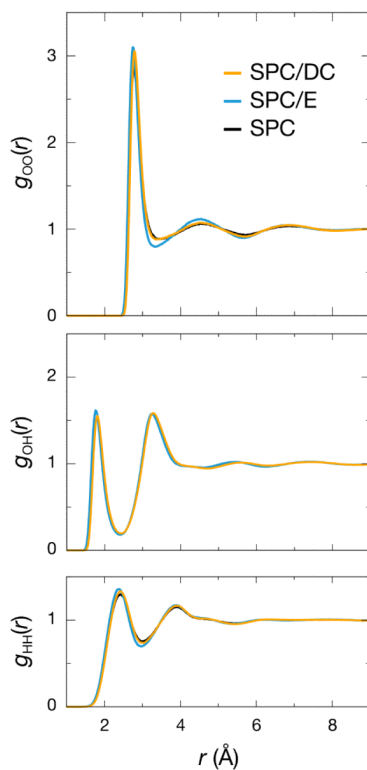


**Figure 7.** The oxygen-oxygen (top), oxygen-hydrogen (middle), and hydrogen-hydrogen (bottom) radial distribution functions for SPC, SPC/E, and SPC/DC. The SPC and SPC/DC curves overlap tightly in all the plots with the only deviations being slightly enhanced peaking in the  $g_{OO}(r)$  and  $g_{HH}(r)$ .

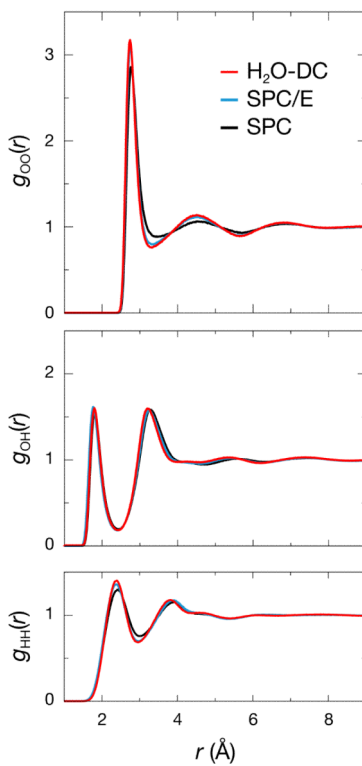


**Figure 8.** The oxygen-oxygen (top), oxygen-hydrogen (middle), and hydrogen-hydrogen (bottom) radial distribution functions for SPC, SPC/E, and H<sub>2</sub>O-DC. The H<sub>2</sub>O-DC model is even more structured than SPC/E, making it a potentially better fit to experimental scattering data.

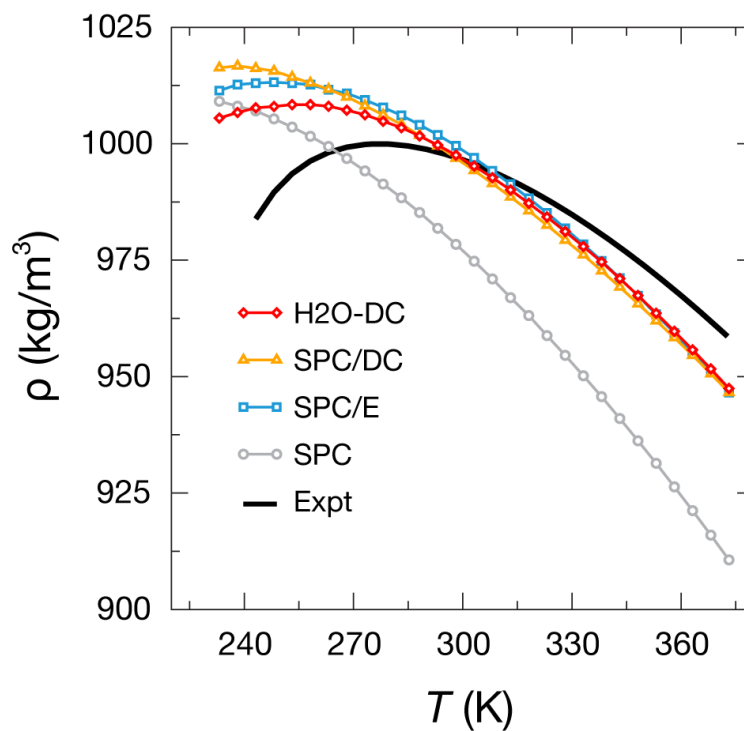


**Figure 9.** The density of the studied water models as a function of temperature. These fully tetrahedral water models all exhibit a density maximum at a lower temperature than real water,<sup>50,51</sup> though geometric differences between the models indicate a route to correct this flaw.

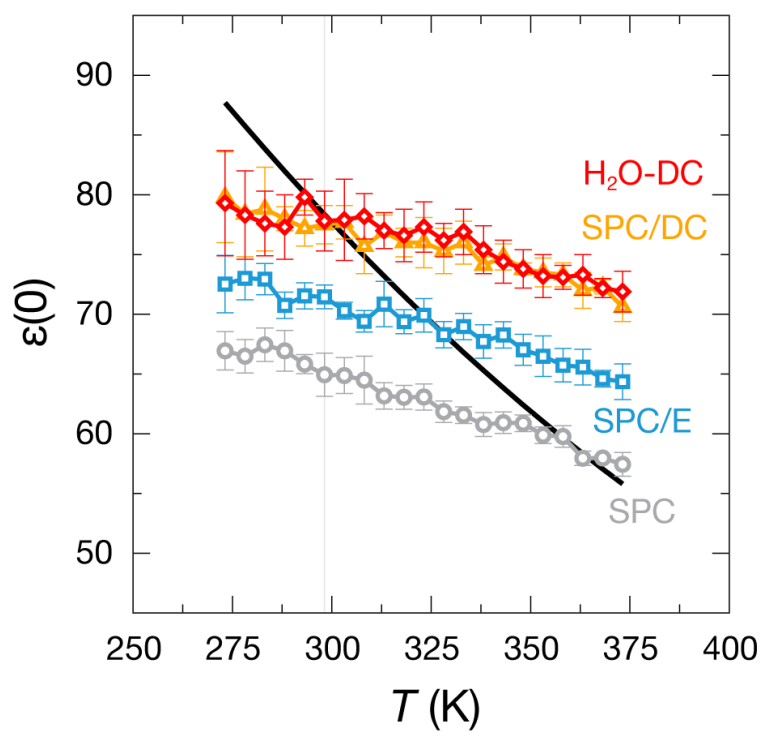


**Figure 10.** The  $\epsilon(0)$  as a function of temperature for the labeled water models alongside experiment<sup>22</sup> (black line). All models capture the trend of decreasing  $\epsilon(0)$  with increasing temperature, though they all fail to reproduce the experimental slope of this trend.

**Table 1**

Experimental properties at 298 K and 1 atm<sup>22</sup> and fitting tolerances for the investigated liquids.

	$\rho$ (kg/m <sup>3</sup> )	tolerance $\pm 2$	$\Delta H_{\text{vap}}$ (kJ/mol)	tolerance $\pm 0.5$	$\epsilon(0)$	tolerance $\pm 0.15$
CCl <sub>4</sub>	1587	$\pm 2$	32.45	$\pm 0.5$	2.23	$\pm 0.15$
CHCl <sub>3</sub>	1473	$\pm 2$	31.30	$\pm 0.5$	4.71	$\pm 0.15$
CH <sub>2</sub> Cl <sub>2</sub>	1317	$\pm 2$	28.82	$\pm 0.5$	8.93	$\pm 0.15$
H <sub>2</sub> O	997	$\pm 2$	43.99	$\pm 0.5$	78.4	$\pm 1.5$

Table 2

Model parameters for CCl<sub>4</sub>-DC with a localized dipole (L), CCl<sub>4</sub>-DC with a distributed dipole (D), CHCl<sub>3</sub>-DC, and CH<sub>2</sub>Cl<sub>2</sub>-DC

Model	Atom-type	Constraint	d (Å)	q (e <sup>-</sup> )	σ (Å)	ε (kJ/mol)
CCl <sub>4</sub> -DC (L)	C			0.14780	4.06640	0.587072
	CL			-0.14780 & 0	4.18602	0.587072
CCl <sub>4</sub> -DC (D)		C-CL	1.7670			
		CL-CL	2.8855			
	C			0.22542	4.06830	0.585791
	CL			-0.07514 & 0	4.18796	0.585791
CHCl <sub>3</sub> -DC		C-CL	1.7670			
		CL-CL	2.8855			
	UA			0.55179	3.73400	1.078200
	CL			-0.18393	3.58871	1.078200
CH <sub>2</sub> Cl <sub>2</sub> -DC		UA-CL	1.7894			
		CL-CL	2.9028			
	UA			0.40440	3.71813	1.281890
	CL			-0.20220	3.53079	1.281890
		UA-CL	1.8215			
		CL-CL	2.9344			

Table 3

Liquid properties for chloromethanes calculated at 298.15 K and 1 atm with standard error of the last digit in parentheses

Liquid	Model	$\rho$ (kg/m <sup>3</sup> )	$\Delta H_{\text{vap}}$ (kJ/mol)	$\epsilon(0)$	$C_p$ (J/mol·K)	$\kappa_T$ (10 <sup>5</sup> atm <sup>-1</sup> )	$\alpha_p$ (10 <sup>6</sup> K <sup>-1</sup> )	$D$ (10 <sup>-9</sup> m <sup>2</sup> /s)	$\mu$ (D)
CCl <sub>4</sub>	CCl <sub>4</sub> -DC (L)	1588.7 (1)	32.392 (3)	2.202 (6)	154 (2)	134 (2)	213 (4)	1.24 (2)	1.26
	CCl <sub>4</sub> -DC (D)	1588.77 (7)	32.406 (1)	2.112 (8)	156 (2)	137 (2)	219 (4)	1.26 (3)	1.23
Fox		1626.6 (5)	34.51 (1)	1.0302 (2)	120 (1)	102 (3)	126 (3)	1.73 (3)	0.23
	Expt	1587 <sup>d</sup>	32.43 <sup>d</sup>	2.228 <sup>a</sup>	130.7 <sup>a</sup>	111 <sup>b</sup>	116 <sup>b</sup>	1.4 <sup>c</sup>	
CHCl <sub>3</sub>	CHCl <sub>3</sub> -DC	1471.16 (7)	31.222 (4)	4.77 (3)	85 (1)	78 (2)	116 (2)	1.48 (3)	1.66
	Fox	1476.7 (2)	30.119 (6)	4.39 (1)	118 (1)	121 (4)	244 (5)	2.74 (8)	1.40
CH <sub>2</sub> Cl <sub>2</sub>	Expt	1473 <sup>d</sup>	31.28 <sup>d</sup>	4.711 <sup>d</sup>	114.2 <sup>a</sup>	106 <sup>b</sup>	123 <sup>b</sup>	2.3 <sup>d</sup> , 2.5 <sup>e</sup>	
	CH <sub>2</sub> Cl <sub>2</sub> -DC	1316.34 (1)	28.740 (1)	8.8 (1)	92.3 (8)	98 (1)	159 (2)	2.13 (2)	2.10
Fox		1265.9 (4)	25.95 (1)	8.65 (3)	118 (1)	158 (1)	180 (2)	4.11 (5)	2.01
	Expt	1317 <sup>d</sup>	28.82 <sup>d</sup>	8.93 <sup>d</sup>	101.2 <sup>a</sup>	104 <sup>a</sup>	139 <sup>a</sup>	3.3 (2) <sup>f</sup>	

<sup>a</sup>Reference 22

<sup>b</sup>Interpolated to 298.15 K from data in Reference 22

<sup>c</sup>Reference 34

<sup>d</sup>Reference 35

<sup>e</sup>Reference 36

<sup>f</sup>Reference 37



Table 4

Model parameters for SPC/DC and H<sub>2</sub>O-DC

Model	Atom-type	Constraint	$d$ (Å)	$q$ (e <sup>-</sup> )	$\sigma$ (Å)	$\epsilon$ (kJ/mol)
SPC/DC	O			-0.87362	3.15767	0.822882
	H			0.43681	0.00000	0.000000
H <sub>2</sub> O-DC		O-H	1.00000			
		H-H	1.63299			
	O			-0.90990	3.18400	0.593000
	H			0.45495	0.00000	0.000000
		O-H	0.95800			
		H-H	1.56441			

Table 5

Liquid properties for water calculated at 298.15 K and 1 atm with standard error of the last digit in parentheses

Model	$\rho$ (kg/m <sup>3</sup> )	$DH_{\text{vap}}$ (kJ/mol)	$\epsilon(0)$	$C_p$ (J/mol·K)	$\kappa_T$ (10 <sup>5</sup> atm <sup>-1</sup> )	$\alpha_p$ (10 <sup>6</sup> K <sup>-1</sup> )	$D$ (10 <sup>-9</sup> m <sup>2</sup> /s)	$\mu$ (D)
SPC	978.41 (3)	36.820 (1)	65.6 (2)	82.9 (3)	53.7 (5)	71.5 (7)	3.99 (1)	2.27
SPC/E	999.53 (2)	41.905 (1)	71.1 (1)	86.3 (2)	46.1 (2)	49.1 (4)	2.46 (1)	2.35
SPC/DC	998.69 (2)	43.993 (1)	78.3 (6)	83.2 (3)	43.7 (3)	48.8 (9)	2.48 (1)	2.42
H <sub>2</sub> O-DC	997.55 (2)	43.366 (1)	78.7 (6)	87.8 (2)	45.0 (2)	44.8 (4)	2.17 (1)	2.42
Expt	997.5 <sup>a</sup>	43.99 <sup>a</sup>	78.36 <sup>a</sup>	75.3 <sup>a</sup>	45.84 <sup>a</sup>	25.6 <sup>a</sup>	2.299 <sup>b</sup>	

<sup>a</sup>Reference 22

<sup>b</sup>Reference 43